Mon. Not. R. Astron. Soc. **380,** 1285–1296 (2007) doi:10.1111/j.1365-2966.2007.12182.x

Lithium in LP 944−20⋆

Ya. V. Pavlenko,[1,2]† H. R. A. Jones,[2] E. L. Martín,[3,4] E. Guenther,[5] M. A. Kenworthy[6] and M. R. Zapatero Osorio[3]

[1]*Centre for Astrophysics Research, University of Hertfordshire, College Lane, Hatfield, Hertfordshire AL10 9AB*
[2]*Main Astronomical Observatory, Academy of Sciences of the Ukraine, Golosiiv Woods, Kyiv-127, 03680 Ukraine*
[3]*Instituto de Astrofí sica de Canarias, La Laguna, Tenerife 38200, Spain*
[4]*Department of Physics, University of Central Florida, PO Box 162385, Orlando, FL 32816, USA*
[5]*Thüringer Landessternwarte Tautenburg, 07778 Tautenburg, Germany*
[6]*CAAO, Steward Observatory, 933 N.Cherry Ave, Tuscon, AZ 85721, USA*

Accepted 2007 July 3. Received 2007 May 18; in original form 2006 October 2

ABSTRACT

We present a new estimate of the lithium abundance in the atmosphere of the brown dwarf LP 944−20. Our analysis is based on a self-consistent analysis of low-, intermediate- and high-resolution optical and near-infrared spectra. We obtain $\log N(\mathrm{Li}) = 3.25 \pm 0.25$ using fits of our synthetic spectra to the Li I resonance line doublet profiles observed with Very Large Telescope/Ultraviolet–Visual Echelle Spectrograph (VLT/UVES) and Anglo-Australian Telescope/Segmented Pupil/Image Reformatting Array of Lenslets (AAT/SPIRAL). This lithium abundance is over two orders of magnitude larger than previous estimates in the literature. In order to obtain good fits of the resonance lines of K I and Rb I and better fits to the TiO molecular absorption around the Li I resonance line, we invoke a semi-empirical model atmosphere with the dusty clouds located above the photosphere. The lithium abundance, however, is not changed by the effects of the dusty clouds. We discuss the implications of our estimate of the lithium abundance in LP 944−20 for the understanding of the properties of this benchmark brown dwarf.

Key words: stars: abundances – stars: evolution – stars: fundamental parameters – stars: individual: LP 944−20 – stars: late-type – stars: low-mass, brown dwarfs.

1 INTRODUCTION

M dwarfs are of special interest to many branches of modern astrophysics. The population of these numerous low-mass stars ($M \lesssim 0.6\,\mathrm{M}_{\odot}$) can contain an appreciable amount of the baryonic matter in the Galaxy. The coolest M dwarfs (later than M6) could be young brown dwarfs (Martín, Rebolo & Zapatero Osorio 1996) if they are young enough. The existence of brown dwarfs was predicted by Kumar (1962a,b) and Hayashi & Nakano (1963). The first unambiguous brown dwarfs Teide 1 and Gliese 229B were reported by Rebolo, Zapatero-Osorio & Martín (1995) and Nakajima et al. (1995), respectively.

The 'Lithium test' observation of the Li I resonance doublet at λ670.8 nm was proposed by Rebolo, Martín & Magazzu (1992) and developed by Magazzù, Martín & Rebolo (1993) to distinguish young brown dwarfs from very low-mass stars. This test has allowed the identification of many brown dwarfs of spectral classes M and L (Rebolo et al. 1996; Martín et al. 1997, 1999; Kirkpatrick et al. 1999).

Because of the low temperatures in the cores of brown dwarfs of masses $M < 55\,M_{\mathrm{Jup}}$ lithium is not destroyed. From $55\,M_{\mathrm{Jup}} < M < 75\,M_{\mathrm{Jup}}$, lithium is destroyed on time-scales that can be used to obtain nuclear ages for these very low-mass objects (e.g. Chabrier et al. 2000). However, the application of the lithium test requires improvement of our knowledge about the physics of atmospheres in low-temperature regimes (Pavlenko et al. 1995).

LP 944−20 (other names are APMPM J0340−3526, BRI B0337−3535, LEHPM 3451, 2MASS WJ0339352−352544) is an archetypical brown dwarf of spectral type M9. A dim red dwarf-like star, Luyten Palomar (LP) 944−20 (M9 V) was catalogued by Luyten & Kowal (1975), and the SIMBAD data base lists more than 125 references for this object up to 2007 May. It is interesting to note that it is comparatively bright ($M_{\mathrm{bol}} = 14.22$; Dahn et al. 2002) and also appears to be a young object, a fact that is confirmed by the lithium detection of Tinney (1998).

Using evolutionary tracks Tinney (1998) estimated the age of LP 944−20 to be between 475 and 650 Myr. Ribas (2003) found

⋆Based on observations obtained on the European Southern Observatory at Cerro Paranal, Chile, in programs 68.C-0063(A) and 072.C-0110(B), the Anglo-Australian Telescope at Siding Springs Observatory during commissioning observations for SPIRAL (Segmented Pupil/Image Reformatting Array of Lenslets) instrument and the Keck Observatory in Mauna Kea, Hawaii.

†E-mail: yp@mao.kiev.ua

some evidence for the membership of LP 944−20 in the Castor moving group in the solar vicinity ($R \sim 5-20$ pc from the Sun). The age of LP 944−20 as a member of the Castor group LP 922−20 has been estimated as 320 ± 80 Myr (Ribas 2003).

An unexpectedly strong, solar-like X-ray flare ($\log L_x/L_{bol} = -4.1$) of duration ∼2 h was registered by *Chandra* (Rutledge et al. 2000), but later *XMM–Newton* observations by Martín & Bouy (2002) did not detect any X-ray activity. The quiescent X-ray luminosity of LP 944−20 is lower than that of the active Sun, and X-ray flares on LP 944−20 are very rare events in comparison with more massive M dwarfs (Hambaryan et al. 2004). However, LP 944−20 is not the only M9 dwarf showing X-ray flares. Recently, Stelzer (2005) observed an X-ray flare ($\log L_x/L_{bol} = -3.3$) from the brown dwarf binary with spectral types M8.5/M9 Gl569 B, which has an age of about 300 Myr (Zapatero Osorio et al. 2004, see also Viti & Jones 1999).

Our knowledge about the structure of the outermost layers of ultracool dwarfs is far from complete (e.g. see discussion in Liebert et al. 2003). Indeed, Berger et al. (2001) reported the discovery of both quiescent and flaring radio emission from LP 944−20. They observed radio luminosities of 80 μJy in quiescence and 2 μJy at flare peak, respectively, which are several orders of magnitude larger than those predicted by the empirical relations between X-ray and radio luminosities that has been found for late-type stars. From the comparison of the continuous and flare fluxes at 8.5 GHz, Berger et al. (2001) concluded that the dwarf has a rather weak magnetic field in comparison with flaring M stars, and its emission mechanism is the most likely non-thermal synchrotron radiation.

Tsuji et al. (1996) predicted 'dusty effects' in the atmospheres of cool dwarfs with $T_{eff} < 2600$ K. The presence of large amounts of dust in the highly dynamical atmospheres of fast rotating ultracool dwarfs can yield 'weather phenomena' (Jones & Tsuji 1997; Gelino et al. 2001; Martín, Zapatero Osorio & Lehto 2001; Clarke, Oppenheimer & Tinney 2002; Bailer-Jones & Lamm 2003; Caballero, Béjar & Rebolo 2003; Koen, Matsunaga & Menzis 2004). LP 944−20 also shows significant rotational broadening in high-resolution spectra. The $v \sin i$ values determined by different authors are in the range of 30 ± 2 km s^{-1} (Tinney & Reid 1998; Guenther & Wuchterl 2003; Mohanty & Basri 2003; Jones et al. 2005; Zapatero Osorio et al. 2006). The rotation period has not been determined yet, but photometric variability was reported by Tinney & Tolley (1999). These surface inhomogeneities could be due to magnetic spots or dusty clouds modulated by stellar rotation.

Tinney (1998) reported the observation of a strong lithium line in the spectrum of LP 944−20 as evidence of its youth and substellar nature, and estimated a lithium abundance of $\log N(\mathrm{Li}) = 0.0 \pm 0.5$, indicating it had depleted an important amount of lithium. This is so far the only determination of the lithium abundance in LP 944−20, which was obtained via comparison of the observed feature width with theoretical curves of growth. However, the observed atomic line at 670.8 nm is measured with respect to the molecular background formed by TiO lines and therefore a detailed spectral analysis needs to be made. Here we present new computations using different approaches and model atmospheres indicating that LP 944−20 has not depleted any lithium.

This paper is organized as follows. Section 2 presents the spectroscopic data of LP 944−20 available in the literature. Section 3 describes the procedure followed to compute synthetic spectra and spectral energy distributions (SEDs) using standard model atmospheres. We fit these theoretical spectra to the observations. In Section 4 we discuss the results obtained in the framework of the conventional approach and we derive a new estimate of the lithium abundance in LP 944−20. In Section 5 we investigate the impact of the possible deviations of physical parameters on our results. We propose a semi-empirical (SE) model for the formation of molecular features and strong resonance lines of alkali elements in the spectrum of LP 944−20. We present the results of applying the SE model for fitting K I, Rb I and Li I lines in high-resolution spectra and SEDs. We derive a new estimate of the lithium abundance in LP 944−20 with our SE model atmosphere, and in Section 6 we discuss the implications of our results.

Coloured versions of plots are available at ftp://star-ftp.herts.ac.uk/pub/Pavlenko/lp944.20

2 OBSERVATIONS

The observed spectra used for this paper have been published elsewhere. In order to simplify the text of the paper we adopt a labelling syntax for them as follows.

(i) *CASPEC*. Optical spectra obtained by Tinney & Reid (1998) using the Cassegrain Echelle Spectrograph (CASPEC) on the European Southern Observatory (ESO) 3.6-m telescope ($R \sim 18\,000$). The infrared part of the SED was obtained by United Kingdom Infrared Telescope (UKIRT; see references in Leggett et al. 2001). The combined spectrum was taken from the Leggett's data base (ftp://ftp.jach.hawaii.edu/pub/ukirt/skl/). We believe Leggett et al. (2001) normalized the spectral data using broad-band photometry but the error on this is of the order of 10 per cent. We have rescaled the flux beyond 1 μm by 10 per cent to improve the match between observed and synthetic spectra.

(ii) *SPIRAL*. Spectra of medium resolution obtained with SPIRAL (Segmented Pupil/Image Reformatting Array of Lenslets) Phase A fibre-fed spectrograph on the Anglo-Australian Telescope (AAT). The full width at half-maximum (FWHM) was typically 2.4 to 2.7 pixel over the whole data, the GFWHM, i.e. FWHM of the smoothing Gaussian, was of order 0.883 Å for the Li I 670.8-nm line ($R = 7500$). See Kenworthy, Parry & Taylor (2001) for the data reduction details.

(iii) *NIRSPEC*. The near-infrared spectrum (NIRSPEC) of LP 944−20 (1.240–1.258 μm, $R \sim 22\,000$) was taken with Keck II. All details about those observations have been published in Martín et al. (2006) and Zapatero Osorio et al. (2006).

(iv) *UVES*. High spectral resolution spectrum obtained with UVES (Ultraviolet–Visual Echelle Spectrograph) on the Very Large Telescope (VLT) Unit Telescope 2 (KUEYEN) at Paranal in service mode. The setting simultaneously covers the wavelength regions from 667.0 to 854.5 nm. We used the average of 15 individual spectra obtained for the purpose of radial velocity monitoring. Details of the data reduction and calibration can be found in Guenther & Wuchterl (2003). The theoretical resolution of our UVES spectra is of order 40 000, corresponding to the GFWHM = 0.17 Å.

3 STANDARD SPECTRAL MODELLING

To determine the surface temperature (T_{eff}) of LP 944−20 we have used the equation $L = 4\pi R^2 \sigma T_{eff}^4$, normalized to solar units. The trigonometric parallax of LP 944−20 is found to be 200.7 ± 4.2 mas, which is the mean value of the measurements obtained by Tinney (1998) and Dahn et al. (2002), yielding a distance of 5.0 pc to the dwarf. By using the bolometric corrections for the J and K bands and the observed near-infrared photometry of LP 944−20 available in the literature, we have derived its luminosity at $\log L/L_\odot = -3.79 \pm 0.03$, which is in agreement with the previous

determination by Dahn et al. (2002). The error bar accounts for the uncertainties in the photometry, bolometric corrections and parallax.

The radii of 'old' ($\geqslant$500 Myr) brown dwarfs are nearly independent of mass and age, with a mean radius of 0.09 $R_\odot$ (see Burgasser 2001), we derive $T_{\rm eff} = 2170$ K. However, the fact that lithium is indeed detected in the optical spectrum of LP 944−20 indicates that this object is significantly younger than other field dwarfs of similar classification, which do not show the lithium feature in absorption. Tinney (1998) and Ribas (2003) state that the age of LP 944−20 is in the range 240–650 Myr, with a likely value at 320 Myr. For such a young age, recent evolutionary models predict brown dwarf (0.05−0.07 $M_\odot$) radii of about 0.10 $R_\odot$ (Burrows et al. 1997; Chabrier & Baraffe 2000), i.e. 11 per cent larger than typical field brown dwarfs. This yields a temperature $T_{\rm eff} = 2040$ K, which is the value that we will use throughout the present paper. Recently, Bihain et al. (2006) have shown that proper motion Pleiades brown dwarfs may have radii similar to those of much older substellar objects, suggesting that brown dwarfs collapse faster than expected. To account for this, we estimate the uncertainty in our $T_{\rm eff}$ determination of LP 944−20 to be $\pm$150 K, which includes the luminosity error bar and the various object sizes valid for an age interval 120–1000 Myr.

Our strategy is divided into the following steps. (i) Theoretical spectra are computed and fitted to the observed SED of LP 944−20 from 0.65 to 2.5 μm. (ii) We then compare our synthetic spectra obtained following a standard classical approach with some atomic and molecular features in the observed spectrum (in particular, the resonance lines of K I, Rb I). Here we use spectra of medium and high spectral resolution. Finally, (iii) we determine the sensitivity of our best-fitting lithium abundance to the input parameters of our models.

3.1 Synthetic spectra

Theoretical SEDs (hereafter we use the term 'synthetic spectra') were computed for model atmospheres of dwarfs with effective temperatures $T_{\rm eff} = 1800-2400$ K and $\log g = 4.0-4.5$ cm s^{-2} from the DUSTY and COND model atmospheres (Allard et al. 2001) of solar metallicity (Anders & Grevesse 1989). Hereafter we use the model atmosphere notation 2400/4.5/0.0 to mean $T_{\rm eff} = 2400$ K, $\log g = 4.5$, [M/H] = 0. We will focus on results obtained with 2000/4.5/0 model atmosphere because as previously indicated, 2040 K is an appropriate effective temperature of LP 944−20, and $\log g = 4.5$ since LP 944−20 is considered to be younger than field dwarfs of similar classification. Nevertheless, computed spectra for other temperatures and gravities were used to study the dependence of our results on these parameters.

The dominant opacity sources in the optical and infrared spectra of LP 944−20 are absorption by band systems of diatomic molecules, such as TiO and VO. Computations of synthetic spectra were carried out by the program WITA5 (Pavlenko, Zapatero Osorio & Rebolo 2000) assuming local thermodynamical equilibrium (LTE), hydrostatic equilibrium for a one-dimensional model atmosphere and without sources and sinks of energy. The equations of ionization-dissociation equilibrium were solved for media consisting of atoms, ions and molecules. We took into account ∼100 components (Pavlenko 1998b). The constants for the equations of chemical balance were taken mainly from Tsuji (1973) and Gurvitz, Weitz & Medvedev (1989).

Our lithium containing species list includes Li I, Li I, LiOH, LiH, LiF, LiBr, LiCl. Our computations show that within our ($T_{\rm eff}$, $\log g$) range neutral lithium dominates across the atmospheres – only 5 per cent of lithium atoms are bound in molecules in the outermost layers of atmosphere (Fig. 1). The most abundant lithium containing species are molecules of LiCl (in the outermost layers) as well as Li I and LiOH (in the photospheric layers).

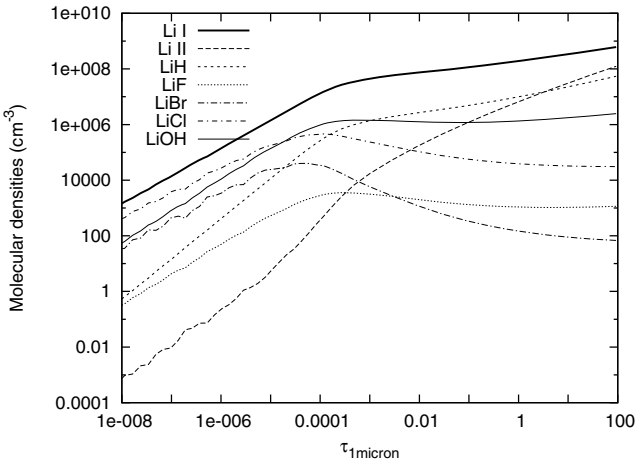

Figure 1. Molecular densities of lithium containing species in the 2000/4.5/0.0 model atmosphere ($T_{\rm eff} = 2000$ K, $\log g = 4.5$, solar metallicity).

3.2 Molecular and atomic lines opacity

The molecular line data are taken from different sources: TiO line lists by Plez (1998); CN lines from CD-ROM 18 (Kurucz 1993); CrH and FeH lines from Burrows, Ram & Bernath (2002b) and Dulick, Bauschlincher & Burrows (2003), respectively. Atomic line list data are taken from Vienna Atomic Line Database (VALD; Kupka et al. 1999).

The profiles of molecular and atomic lines are determined using the Voigt function $H(a, v)$ except for the strong resonance doublet lines of Na I (0.5891, 0.5897 μm) and K I (0.7667, 0.7701 μm) (see Section 3.4). The parameters of natural broadening C_2 and van der Waals broadening C_6 of absorption lines are taken from Kupka et al. (1999), or in their absence computed following Unsöld (1955). In our computations we used a correction factor E for van der Waals broadening of atomic lines. Parameter E describes differences in broadening parameters computed in the framework of classical and quantum physics approaches. For resonance lines of alkali metals $E = 1-2$ (see Andretta, Gomez & Severino 1991). Owing to the low electron and ion densities in low temperature M dwarf atmospheres, Stark broadening may be neglected. In general the effects of pressure broadening prevail. Computations for synthetic spectra to be fitted to observed spectra across the 0.65–0.9 μm are carried out at intervals of 0.5 Å. For comparison with high-resolution spectra we computed spectra with an interval of 0.02 Å. The spectrum broadening is modelled by Gaussian plus rotational profiles set to the resolution of the observed spectra. Rotational broadening was taken into account following the Gray (1976) formulae with $v \sin i = 30$ km s^{-1} (see Jones et al. 2005). VO band opacity is computed in the frame of the JOLA (just overlapping line approximation) (see Pavlenko et al. 2000, for more details). The relative importance of the different opacities contributing to our synthetic spectra is shown in Fig. 2.

In this paper we also pay careful attention to the modelling of the rubidium resonance line at 780.2 nm. Resonance lines of Rb I have superfine structure (Lambert & Mallia 1968; Lambert & Luck 1976),

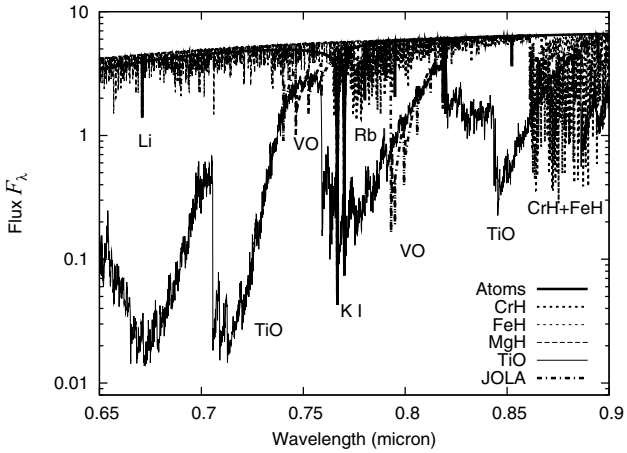

Figure 2. A plot identifying the main features in a 2400/4.5/0.0 model spectrum, showing their relative strengths.

which is important to account when considering weak absorption lines, but the Rb I lines in our spectra are strong. Moreover, they are broadened by rotation and turbulent motions and so the superfine splitting of Rb I lines can be neglected (see Lambert & Mallia 1968; Lambert & Luck 1976). We assume that all atoms of rubidium are the ^{58}Rb isotope. Most features of the observed spectra should be fitted using the same atmospheric parameters of temperature and gravity. We will use our fits to the Rb I line as a test of the consistency of our spectroscopically derived results to $\log g$ and lithium abundance in the atmosphere of LP 944−20.

3.3 Observed profiles of Li I and Rb I

The flux variations across Li I and Rb I line regions obtained in a few separate observing runs are shown in Fig. 3. We show there a sequence of the first five observed fluxes from a set of 15 spectra which were used to get the combined spectrum used in our analysis. It is worth noting that changes in the Rb I line 780.2-nm profile are rather small. However, we see here some variations in molecular background formed by the haze of TiO lines. In general, the response of the TiO molecular densities to changing temperatures in the line-forming region should be much higher in comparison with changes of the ionization equilibrium of alkali metals (see Pavlenko 1998a). Some variations of the observed fluxes across the 780-nm region are real. Analysis of the topic is beyond the scope of our paper.

For the 670-nm region, we find that the data from individual UVES epochs appear to be reasonably fit, albeit at low signal-to-noise ratio, by the same parameters as the higher signal-to-noise ratio Rb lines. However, when the data set is combined (15 low signal-to-noise ratio epochs spread over more than a year) a considerably broader Li I profile results. This is not due to radial velocity changes for which this data set has already being corrected to a level of the order of 80 m s^{-1} (Guenther & Wuchterl 2003). This apparently changing line profile is presumably due to either variability and/or relatively low signal-to-noise ratio of the UVES data at these wavelengths and leads us to fit the combined profile with a lower effective resolution. We find the lithium region to be best fit with $v \sin i = 32$ km s^{-1} and a GFWHM = 1 Å.

3.4 K and Na resonance lines

In the spectra of ultracool dwarfs the resonance lines of Na I and K I are very strong. They govern the SEDs of L dwarfs across a wide spectral region (see Pavlenko 2001, for more details). Their formally computed equivalent widths (EWs) may be of the order of a few thousand Å. For these features we cannot use a classical collisional approach to compute the wings of these superstrong lines. In the dense, cool atmospheres of late M, L and T dwarfs the pressure broadening of K I and Na I can be computed with a quantum chemical approach (Allard et al. 2003; Burrows & Volobuyev 2003).

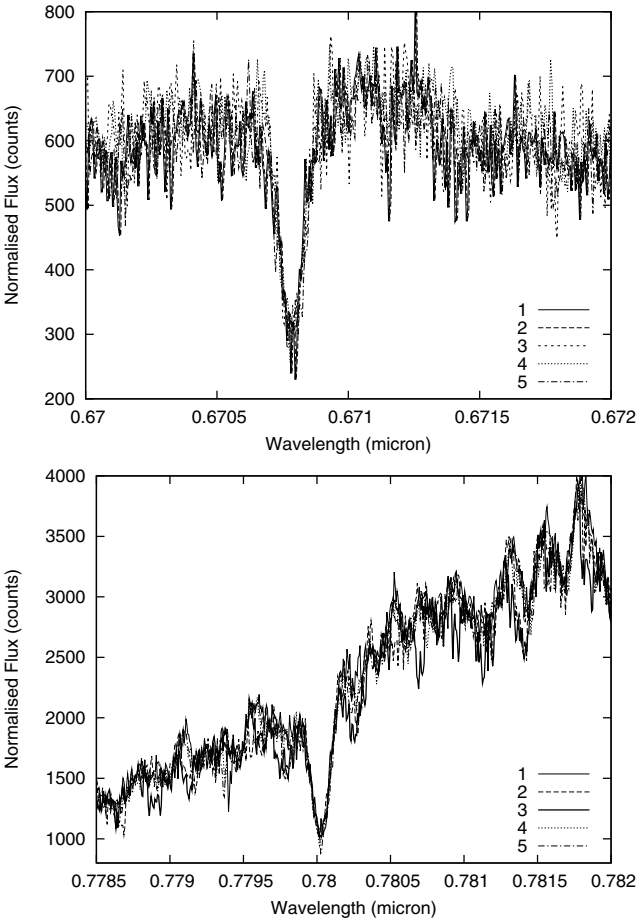

Figure 3. Observed fluxes of LP 944−20 for the first five (in chronological order) UVES echelle orders across spectral regions containing Li I and Rb I resonance lines.

For this work we use potentials of quasi-stationary chemical interactions of atoms K and Na with the most numerous species, i.e. atoms He and molecules H_2 computed by GAMESS (Granovsky et al. 1999). Our procedure is described in more detail in Pavlenko, Zhukovska & Volobuyev (2007). Here we point out that in computations of K I profiles we used a combined profile: cores of these lines were computed in the frame of the collisional approach, and their wings ($\delta\lambda > 40$ Å) were treated by quasi-stationary theory. It is worth noting that K and Na lines have comparatively weak wings in our range of $T_{\rm eff}$ and $\log g$. Thus, in observed spectra we see only cores of strong absorption lines against a background of molecular bands.

For other alkali lines we used a conventional, i.e. collisional theory of pressure broadening, using van der Waals formulae for computation of damping constants described in Pavlenko (2001). The relative strength of the resonance lines of neutral alkali lines is shown in Fig. 2.

3.5 Fit to the observed spectral energy distribution

To get the best fits of our theoretical spectra to the observed SED, we followed the scheme described in Pavlenko et al. (2006) and references therein. Namely, we find the minimum value of the following equation:

$$S(f_{\rm h},\, f_{\rm s},\, f_{\rm g}) = \Sigma \left(f_{\rm h}\, H^{\rm synt} - H^{\rm obs} \right)^2. \quad (1)$$

Here $H^{\rm obs}$ and $H^{\rm synt}$ are observed and computed fluxes, $f_{\rm h}$ is a normalization parameter, $f_{\rm s}$ is the relative wavelength shift of the observed spectra and $f_{\rm g}$ is related to the broadening parameters. In our case, we applied both rotational and instrumental broadening. These were modelled by Gray (1976) formulae (rotational broadening) and Gaussian functions (instrumental broadening).

4 RESULTS BASED ON STANDARD SPECTRAL MODELLING

4.1 Fit to the observed spectral energy distributions

In Fig. 4 we show fits to the observed SEDs of LP 994−20 across the 0.65–2.5 μm region. We carried out our fits for the DUSTY and COND model atmospheres. We exclude from the fitting the spectral region 0.86–1.96 μm because there is a gap in the observed spectrum, and strong spectral features formed by absorption of H_2O and other molecules at these wavelengths cannot be fitted properly even for the objects of higher $T_{\rm eff}$ (Pavlenko et al. 2006). None the less, our approach allows us to use the optical region governed by TiO bands where flux is very sensitive to $T_{\rm eff}$, and the region beyond 1.96 μm dominated by H_2O and CO bands. Line lists of these molecules for the latter region is of high quality (Pavlenko & Jones 1992; Jones et al. 2002). In general, fits of our theoretical spectra computed with DUSTY model atmospheres to the observed spectra look better. In Fig. 5 we show values of min S computed for a grid of DUSTY and COND model atmospheres. It is worth noting the following.

(i) The values of S are smaller for the DUSTY models across a wide range of effective temperature and gravity, particularly below 2300 K.

(ii) We get min S at $T_{\rm eff} = 2000-2200$ K for the COND models. This result derived through spectral analysis is consistent with our estimation of the surface temperature for LP 944−20 obtained in Section 3 using radii predicted by substellar evolutionary models, the object's astrometry and broad-band photometry.

(iii) Temperatures in the outermost layers of the DUSTY models are higher in comparison with the COND models. As s result for the DUSTY models, S appears to decrease even for $T_{\rm eff} < 2000$ K.

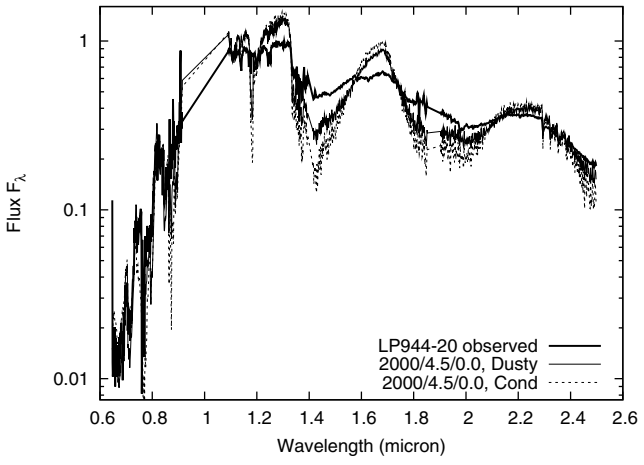

Figure 4. Fits of the synthetic spectra computed for DUSTY and COND model atmospheres 2000/4.5/0.0 to the observed SED of LP 944−20. There is no data between 0.9 and 1.1 μm.

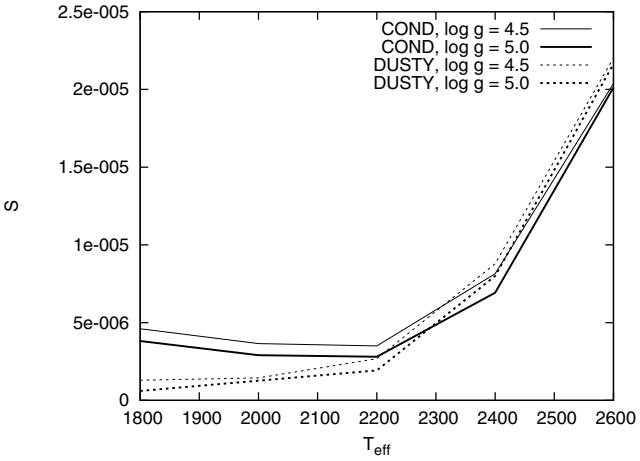

Figure 5. Values of min (S) computed for a grid of DUSTY and COND model atmospheres in the 'standard' framework.

We note that any spectral analysis is affected by uncertainties associated with the adopted structure of model atmospheres, molecular opacities and non-classical effects like the presence of a chromosphere, veiling etc. Additionally, the fits shown in Fig. 4 do not provide a good match to the observed SED of LP 944−20. Therefore, these results should be understood as a qualitative confirmation of the $T_{\rm eff}$ that we have assumed for LP 944−20. From Fig. 4, it becomes apparent that additional parameters describing the atmosphere of LP 944−20 are needed to obtain a better reproduction of the observed data. We will further discuss on this in Section 5. Next, we will show the results for the high-resolution 'standard' analysis.

4.2 Resonance lines of K I and Rb I

Resonance doublets of K I and Rb I are recorded simultaneously. This provides the opportunity to study these lines at a single epoch. The comparison of CASPEC, SPIRAL and UVES spectra shows all these data agree well in spectral slope, widths and intensities of lines. The fits to K I and Rb I resonance line are shown in Fig. 6. The Rb I line is more suitable for analysis, because it is less saturated than the K I doublet. We can fit our synthetic spectra to the observed Rb I profile taking into account the rotation velocity $v \sin i = 30\,{\rm km\,s^{-1}}$ and GFHWM = 0.17 Å (see the bottom panel of Fig. 6). Note that other features mainly due to molecular absorptions of TiO and VO are not so well reproduced in intensity by the models. Nevertheless, the $T_{\rm eff} = 2000$ K and $\log g = 4.5$ model nicely fits the K I and Rb I resonance profiles. We note that higher gravities do not provide a better match to the observed profiles of the alkalis (they predict stronger lines), as we will show next.

Rubidium in LP 944−20 was also studied by Basri et al. (2000). These authors derived $T_{\rm eff} = 2600$ K from the spectral fitting of the Rb I resonance lines. However, Basri et al. (2000) point out that their spectral analysis of the Rb I lines indicates higher temperatures than their analysis of caesium lines (2400 K). Our computations for 2400 K do not provide fits to the SED of LP 944−20 as acceptable as those computed for 2000–2200 K (see Fig. 5). LP 944−20 is

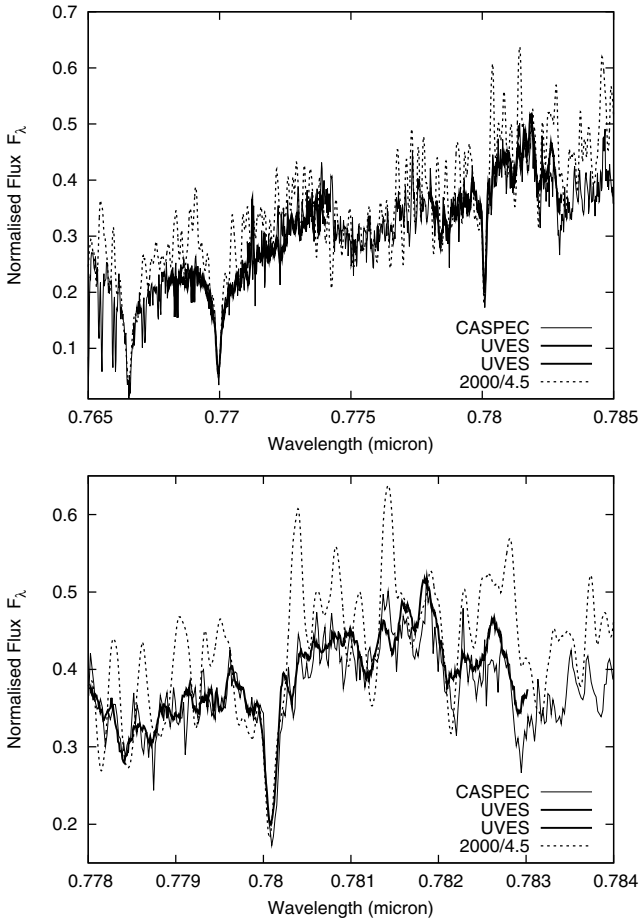

Figure 6. Fits to the K I and Rb I resonance lines observed in the spectra of LP 944−20 following the 'standard' approach. The bottom panel shows an enlargement around the Rb I line. Theoretical spectrum has solar metallicity.

classified as an M9 V field brown dwarf in the literature, thus it shares the same spectral classification as LHS 2924, which was also included in the sample of Basri et al. (2000). These authors found that LP 944−20 is cooler than LHS 2924 in agreement with the more recent results of Dahn et al. (2002), who determine $T_{\rm eff} = 2367$ and 2138 K for LHS 2924 and LP 944−20, respectively. This value is in good agreement with our adopted $T_{\rm eff}$ for the young brown dwarf. We note that our synthetic spectra provide reasonable fits to the observed profiles of all alkali lines in LP 944−20 using the same atmospheric parameters, i.e. without the need of different values of temperature and gravity for the various lines present in the spectra.

4.3 Near-infrared doublet of K I

We have also fit the NIRSPEC spectrum of LP 944−20, which contains the subordinate lines of K I at 1.2432 and 1.2522 μm. These lines turn out to be gravity-sensitive features as observationally shown by McGovern et al. (2004). Their excitation potentials are rather low (∼1.610 eV), thus they can be used for the analysis of stellar spectra. Our fits to the observed profiles of K I subordinate doublet using the standard modelling procedure are shown in Fig. 7. The molecular background at these wavelengths is dominated by absorption of H_2O; CrH and FeH contribute to the opacity as well. Unfortunately, good quality line lists for CrH and FeH do not exist.

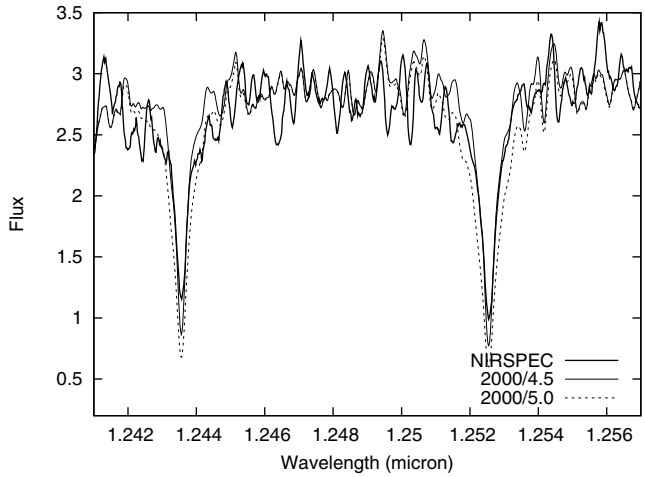

Figure 7. Fits of DUSTY synthetic spectra (solar metallicity, 'standard' approach) to the observed infrared K I subordinate doublet lines.

None the less, we get a good fit to the observed profiles of these lines (Fig. 7) using $T_{\rm eff} = 2000$ K and $\log g = 4.5$. Note that higher gravity models deviate significantly from the observations. From the spectral analysis of young M-type objects carried out by Mohanty et al. (2004), these authors pointed out that their derived gravities for the coolest M dwarfs deviate significantly up to 0.75 dex from the isochrone predictions in the sense that measurements are smaller. Our gravity derivation for LP 944−20 also appears to be lower than the prediction of $\log g \sim 5.0$ based on the evolutionary models by Baraffe et al. (2003) and the likely age of the brown dwarf.

While the overall profiles of the near-infrared K I lines are reasonably reproduced by our computations, the cores of the lines in the theoretical spectra are deeper than those in the observed spectra. These differences in the intensity of the line cores of the saturated lines may be explained by non-local thermodynamical equilibrium (NLTE) effects or chromospheric effects. However, other possible physical explanations can be found, especially those related to the depletion of refractory elements into condensates in cool atmospheres (see Section 5).

4.4 Lithium lines and abundances

The relative strength of atomic lines around the Li resonance doublet and TiO bands are shown in Fig. 8. These computations were carried out for two cases to show the dependence of the strength of the Li I line on the presence of TiO: (i) in the first case we only take into account the absorption for atomic lines, and (ii) in the second and more realistic case we also accounted for molecular absorption. While in the former case, analysis of atomic lines can be carried by EW studies, only pseudo-equivalent widths (pEWs), i.e. EWs measured in respect to the local pseudo-continuum formed by molecular and atomic line background, can be obtained from the spectra computed in case (ii) (see also Pavlenko 1997b).

EWs and pEWs of the Li I resonance doublet differ significantly (see Zapatero Osorio et al. 2002; Pavlenko 2005). The computed EW of the Li I feature at 670.8 nm for the DUSTY model atmosphere 2000/4.5/0 and $\log N({\rm Li}) = 0.0$ is 0.54 and 0.58 Å for turbulent velocities of 2 and 3 km s^{-1}, respectively. For $\log N({\rm Li}) = 3.25$ (i.e. cosmic abundance), we obtain much larger EW of 13.5 Å (this theoretical measurement accounts for the broad wings of the doublet ±40 Å from its core). Interestingly, the formally measured pEW

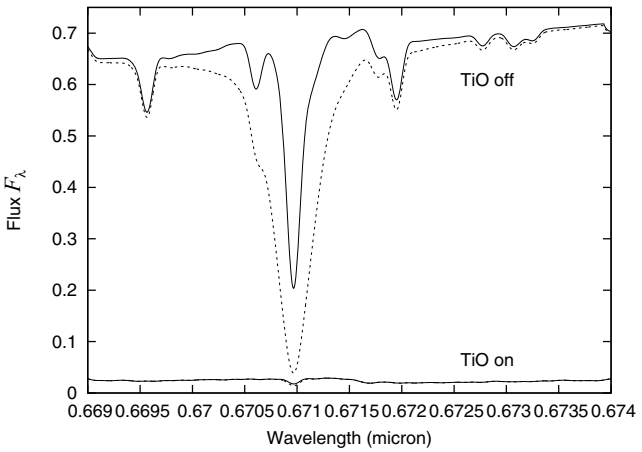

Figure 8. Theoretical profiles of atomic lines in the 670.8-nm region computed both with and without TiO absorption in the 2000/4.5/0.0 model atmosphere. The strongest line is due to Li I. The vacuum scale of wavelengths is used. Synthetic spectra are convolved with GFWHM = 1 Å and $v \sin i = 30\,\mathrm{km\,s^{-1}}$. Solid and dashed lines show spectra computed for $\log N(\mathrm{Li}) = 2.0$ and 3.2, respectively.

of the lithium line obtained for $\log N(\mathrm{Li}) = 3.25$ and the synthetic spectra of case (ii) is considerably smaller, much in agreement with the observations of LP 944−20. Even for case (i) when we only consider atomic absorption lines in our computation of synthetic spectra, we cannot see the extended but weak wings of the lines due to the blending effects by other features.

From the observations of LP 944−20, the pEW of the Li resonance doublet in the UVES spectrum shown in Fig. 9 is 0.65 ± 0.05 Å. Our pEW measurement is consistent with that (pEW $= 0.53 \pm 0.05$ Å) of Tinney (1998), suggesting little variability in the overall strength of the line. We note that these pEWs are very similar to the Li I measurements obtained for σ Orionis members (3 Myr) of related spectral types by Zapatero Osorio et al. (2002). Using curves of growth measured by these authors for the young M dwarfs in σ Orionis (see fig. 16 in Zapatero Osorio et al. 2002), we obtain a lithium abundance of $\log N(\mathrm{Li}) = 3.2 \pm 0.3$ for LP 944−20. Interestingly, the pEW of the Li I line computed for $\log N(\mathrm{Li}) = 3.25$ and derived from the synthetic spectrum shown in Fig. 9 (which accounts for TiO absorption) is 0.65 Å, in agreement with the measurement of LP 944−20.

Nevertheless, synthetic spectra are the most appropriate tool for a reliable lithium line analysis. Fits of our theoretical spectra computed for the DUSTY model atmosphere 2000/4.5/0.0 are shown in Fig. 9; the bottom panel of the figure shows the lithium line in larger scale. Theoretical spectra were computed for several lithium abundances, from depletion by a factor of 10 up to a rich content of $\log N(\mathrm{Li}) = 3.5$. The best fit is provided by $\log N(\mathrm{Li}) = 3.25 \pm 0.25$ (see details in the bottom panel of Fig. 9). LP 944−20 seems to have preserved its original lithium content.

It is worth noting that (i) after appropriate broadening (see Section 3.3) the intensity and profiles of the Li I resonance doublet can be well fit, and (ii) the shape of TiO bands around 670.8 nm cannot be reproduced with standard models. Theoretical spectra predict stronger TiO bands than those observed in LP 944−20 (we note that a change of 0.5 dex in gravity does not have a major impact on the TiO bands in this wavelength range). In the next section we attempt to improve the poor fit to the TiO bands by adjusting our model atmosphere in a manner which seems physically justified.

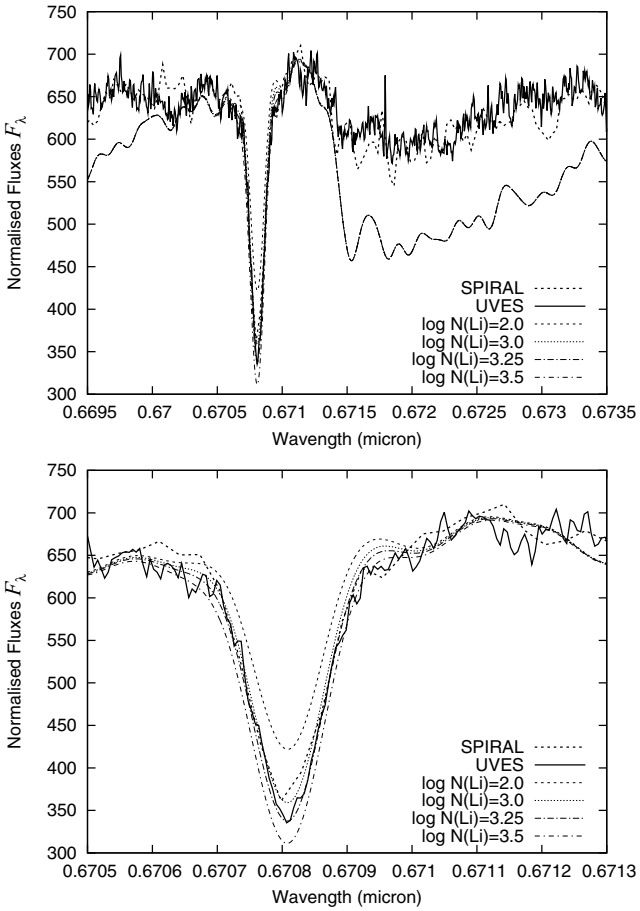

Figure 9. Fits of the lithium 670.8-nm resonance doublet computed for DUSTY model atmosphere 2000/4.5/0.0 and different lithium abundances in the 'standard' framework to observed spectra of LP 944−20. The bottom panel shows an enlargement around the lithium atomic line.

Lithium subordinate lines at 812.6 and 610.3 nm can also be used for Li abundance determination in atmospheres of some lithium-rich late-type stars. Moreover, any abundance derivation becomes more solid if measurements are obtained from as many lithium lines and lithium-bearing species as possible. We find the Li line at 610.3 nm 'sinks' under the TiO bands in the LP 944−20 spectrum. Only the 812.6-nm line can be used for the analysis if reasonably good quality high-resolution spectra were available at these wavelengths. The CASPEC spectrum of LP 944−20 does not comply this requirement. Therefore, in this paper our abundance analysis will be based on the fits to the observed Li I 670.8-nm line profile.

5 ANALYSIS WITH A SEMI-EMPIRICAL MODEL ATMOSPHERE

In the framework of the standard model we have determined the 'cosmic' lithium abundance ($\log N(\mathrm{Li}) = 3.25 \pm 0.25$) in the atmosphere of LP 944−20. The same result was obtained from the spectral analysis of the lithium resonance doublet profile and the study of the line pEW. However, there remain a number of problems. Our fit to the observed SED of LP 944−20 is not adequate in both the optical and infrared regimes. A comparison with high-resolution UVES spectra shows significant differences in the shapes of computed and observed spectra. Namely, the heads of TiO bands look 'smoothed' in the observed spectra. We find our fits obtained

in the framework of the standard model cannot be improved by changes of $T_{\rm eff}$, $\log g$, metallicity or microturbulent velocity.

Generally speaking, these differences reduce the reliability of our analysis, but on the other hand we know dusty effects can affect the temperature structure and spectra of ultracool dwarfs (Tsuji et al. 1996; Jones & Tsuji 1997; Allard et al. 2001; Burrows et al. 2002a, and references therein). Therefore, we construct the new SE model atmosphere. With the new SE model atmosphere we obtain better fits to the overall SED and molecular features around lines of K, Rb and Li resonance doublets. Finally, we redetermine the lithium abundance with the new model atmosphere.

5.1 Semi-empirical model atmosphere

We modified the DUSTY models as follows.

(i) To decrease the intensity of TiO bands in the spectral range 600–800 nm, we suggest the complete absence of TiO above a certain height in the atmosphere of LP 944−20. This can have at least two different physical explanations: (i) the presence of a hot chromospheric-like region in the outermost layers of the dynamical atmosphere, or (ii) the removal of Ti atoms from gaseous species by condensation into dust particles in the upper atmosphere (see Pavlenko 1998b; Ferguson et al. 2005). In our SE model we will explore the latter case, i.e. a depletion of TiO above a particular level in the atmosphere of LP 944−20. Our lower boundary of the depleted TiO is located at the level $\tau_{\rm ross} = 10^{-4}$. The choice of this point has some influence on the absolute values of min S, however, it is not crucial for our results of lithium abundance determination.

(ii) To improve the fits over the wavelength range 0.8–0.9 and 1.6–2.5 μm, we implement additional quasi-continuum opacity (hereafter AqO) provided by dust particles. It is worth noting that dust particles must be present in atmosphere of LP 944−20 due to the low effective temperature of the dwarf. Our knowledge about dust opacity in atmospheres of ultracool dwarfs is rather poor (see, however, review by Ferguson et al. 2005). Here we treat AqO as a scattering with power law dependence on wavelength in the form $a_\lambda = a_0(\lambda_0/\lambda)^N$. We used $\lambda_0 = 0.77$ μm as our reference wavelength. Parameter N varies in the range 0–4. A value of $N = 0$ corresponds to the light scattering by submicron particles ('white scattering'), and $N = 4$ describes Rayleigh scattering.

(iii) In our case, the 'dust opacity' originates in the shell-like structures lying above the photosphere (clouds). It is worth noting that we tried different heights for the location of the 'dusty shell'. The best results are obtained for levels corresponding to $T_{\rm cr} \sim 2000$ K, coinciding with the models of Allard et al. (2001) and Tsuji (2002). These authors refer to $T_{\rm cr}$ as a temperature related to the 'gas–dust' phase transition.

Our scattering dusty cloud structure was modelled by two parameters: thickness of cloud, $\tau_{\rm AqO}$, and the location of the maximum of opacity, $\tau_{\rm d}$. The dusty opacity decreases inward and outwards in the atmosphere with respect to the $\tau_{\rm d}$ point (see Fig. 10) for physical reasons: pressure and density are reduced outwards while temperature increases inwards. These factors naturally decrease the density of the dusty particles at lower and larger optical depths. We vary $\tau_{\rm AqO}$ and $\tau_{\rm d}$ across the ranges 0–1 and 0.001–0.0001, respectively. Note that different locations of the scattering layer correspond in our case to different depths in the atmosphere in which $T = T_{\rm cr}$. Burrows, Sudarsky & Hubeny (2006) have recently proposed a similar model of the dusty cloud with a flat part of the dust distribution located at $T \sim 2300$ K.

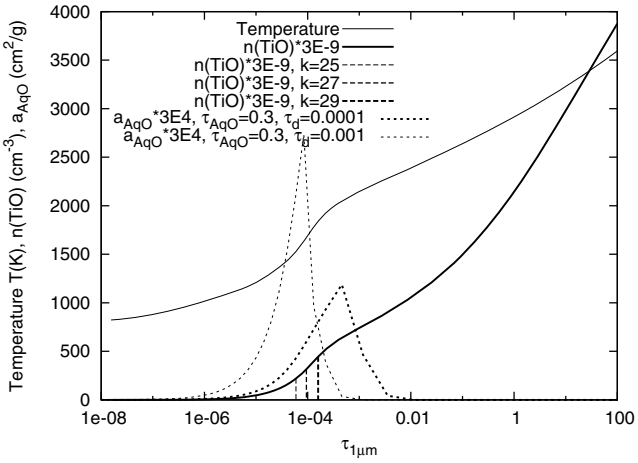

Figure 10. Structures of two SE model atmospheres from our grid.

5.2 Fits to the observed spectral energy distribution

We have computed a grid of theoretical spectra adopting our SE model atmospheres built with different parameters of $\tau_{\rm AqO}$, $\tau_{\rm d}$ and k (k stands for different layers within the atmosphere). A comparison of computed optical and near-infrared SEDs for the SE model atmospheres with AqO ($\tau_{\rm AqO} = 0.9$, $\tau_{\rm d} = 0.001$) and without AqO is shown in Fig. 11. As we see from the comparison, our AqO affects the spectral regions where fluxes are formed in the layers below the level $\tau < \tau_{\rm AqO}$. Strong absorption features formed in the optical spectrum are affected rather marginally. In general, the AqO makes the computed spectra appear 'shallower' than models without AqO, i.e. in agreement with the observations of LP 944−20.

Theoretical SEDs computed for SE model atmospheres were fit to the observed fluxes of LP 944−20 following the procedure described in Section 3.5. It is worth noting the following: (i) the minimization procedure of fits to observed spectra provides lower S for theoretical spectra computed with $N = 0$ (this suggests that the dusty particles present in the modelled dusty cloud structure of LP 944−20 are of submicron size), and (ii) visual comparison of Figs 4 and 12 shows that we get a better fit to the observed SED with theoretical spectra computed with AqO. Analysis of the results of the numerical

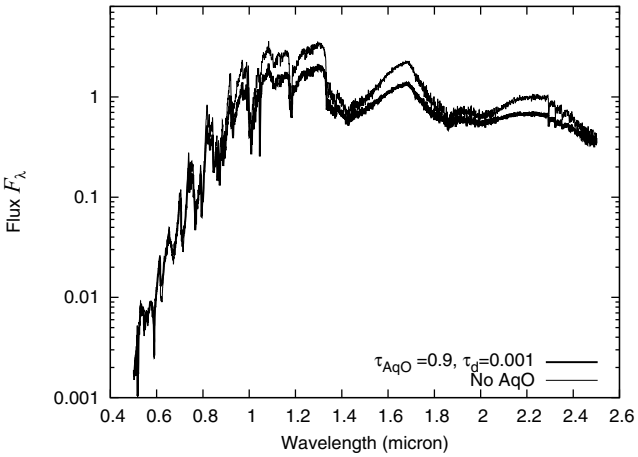

Figure 11. Comparison of fluxes computed with the DUSTY 2000/4.5/0.0 model atmosphere for two different cases: the dust-free atmosphere (no AqO) and the SE model ($\tau_{\rm AqO} = 0.9$, $\tau_{\rm d} = 0.001$, $k = 25$). See also fig. 2 of Burrows et al. (2006).

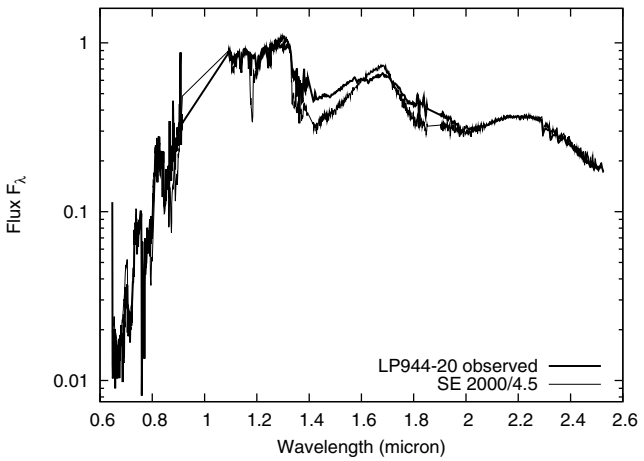

Figure 12. Fit of the theoretical fluxes computed with a SE model atmosphere (2000/4.0/0.0, $\tau_{\rm AqO} = 0.9$, $\tau_{\rm d} = 0.001$, $k = 25$) to the observed SED of LP 944−20. Note the better fit as compared to Fig. 4.

procedure of minimization yields $S = 1.4 \times 10^{-6}$ and 3.9×10^{-7} for the fits shown in Figs 4 (standard approach) and 12 (SE model), respectively. We note that while our SE computations decrease the absolute values of min S, the general shape of the min S dependence on $T_{\rm eff}$ (like the one shown in Fig. 5) is not significantly changed. SE models of $T_{\rm eff} = 2000$ K provide reasonable fits to the observed data of LP 944−20, indicating that our results are stable.

5.3 K I and Rb I resonance lines

Fits of theoretical spectra computed for SE model atmosphere to the spectral region of K I and Rb I lines are shown in Fig. 13. We get even better fits to K I and Rb I resonance lines and to TiO molecular features in terms of intensity in comparison to the dust-free case (see Fig. 6).

5.4 Near-infrared doublet of K I

The NIRSPEC data of LP 944−20 are compared to our synthetic spectrum computed with the SE model atmosphere in Fig. 14. In general, our SE model atmosphere does not have a major impact on the atomic and molecular details of these wavelengths: the fits of the molecular features around K I lines are of the same quality and the profiles of the K I lines are reproduced as in the AqO-free case (see Fig. 7). However, we note that the fits to the observed cores of K I are improved in the AqO model. Again, we see that models of $\log g = 4.5$ provide a much better fit to the atomic lines than higher gravity atmospheres.

5.5 Li I resonance lines

The SPIRAL and UVES spectra of LP 944−20 around Li I 670.8 nm are compared to SE models in Fig. 15. These models have been computed for different lithium abundances, from $\log N({\rm Li}) = 2.0$ up to 3.5. The fits to the resonance line profile of Li I are of similar quality to those depicted in Fig. 9 ('standard models'). However, the TiO absorption fit and the overall fit of the spectral region across the Li resonance doublet is significantly improved in the SE models.

We carry out our lithium abundance determination for the SE model atmosphere. As seen from the bottom panel of Fig. 15, the model computed for $\log N({\rm Li}) = 3.25$ provides the best match to the

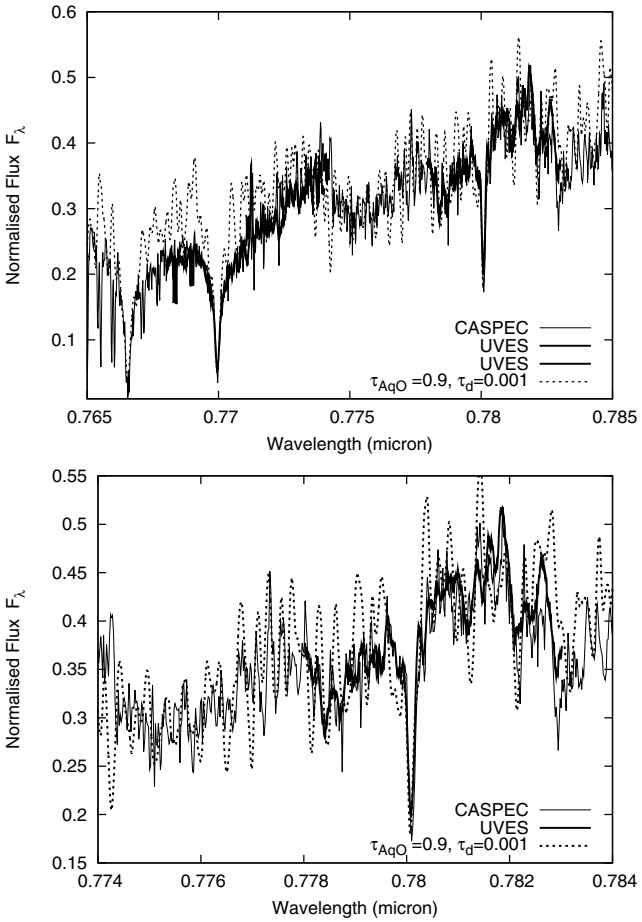

Figure 13. Fits of the synthetic fluxes computed with a SE model atmosphere (2000/4.5/0.0, $\tau_{\rm AqO} = 0.9$, $\tau_{\rm d} = 0.001$, $k = 25$) to the LP 944−20 observed spectrum around K I and Rb I lines. The bottom panel shows an enlargement around the Rb I line.

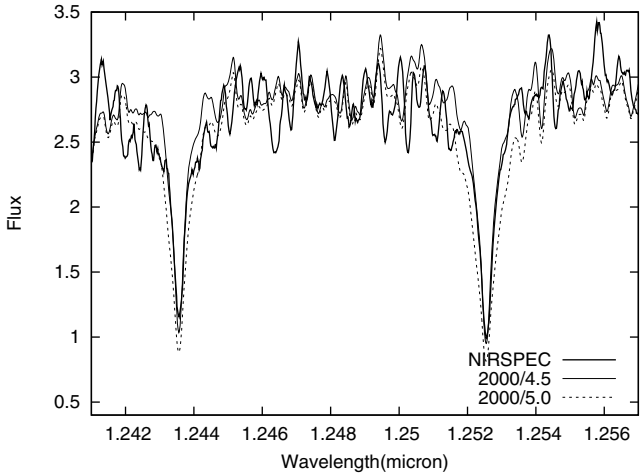

Figure 14. Fit of computed SE models (2000/4.5/0.0 and 2000/5.0/0.0, $\tau_{\rm AqO} = 0.9$, $\tau_{\rm d} = 0.001$, $k = 25$) to the LP 944−20 observed infrared K I subordinate doublet region. The core of the K I lines is better reproduced than in Fig. 7. Note that $\log g = 4.5$ provides a better match to the profiles of these 'gravity-sensitive' atomic lines.

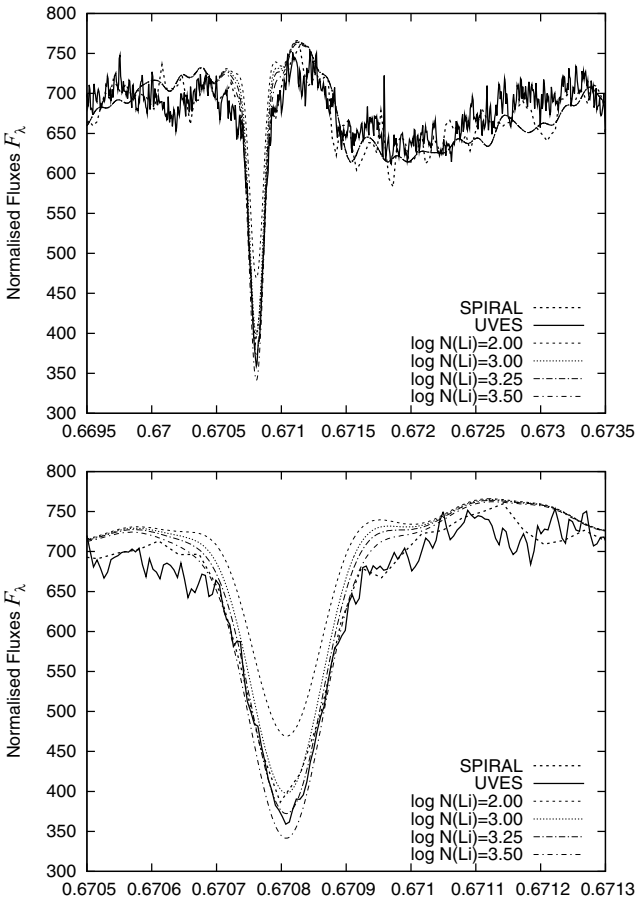

Figure 15. Fits of the theoretical fluxes around Li 670.8-nm resonance doublet computed with SE model atmosphere (2000/4.5/0.0, $\tau_{\rm AqO} = 0.9$, $\tau_{\rm d} = 0.001$, $k = 25$) and different lithium abundances to the observed spectrum of LP 944−20. The bottom panel shows an enlargement around the resonance line. Note the better reproduction of the shape and intensity of the TiO absorption as compared to Fig. 9.

observations. Interestingly, our SE model does not significantly affect the lithium abundance determination for LP 944−20. Observed and theoretical spectra have been normalized over a broad range of wavelengths across the lithium region because the synthetic data provide a reasonable reproduction of the TiO absorption. We have adopted an error bar of ±0.25 dex in our lithium abundance determination; this takes into account the quality of the observed spectra, $T_{\rm eff}$ changes of ±200 K and slight modifications in the normalization of the spectra. From our computations and at the 4σ confidence level we can discard lithium depletion factors larger than 10 in the atmosphere of LP 944−20.

6 DISCUSSION

Our main result has been obtained from the spectral analysis of the high-resolution profile of the Li I doublet resonance line at 670.8 nm using $T_{\rm eff} = 2000$ K ($T_{\rm eff} = 2040$ K is derived for LP 944−20 from photometric and astrometric considerations), $\log g = 4.5$, solar metallicity and different atmospheric lithium contents from depletion of about a factor of 10 up to supercosmic abundance. We also model other alkali lines of K I and Rb I located in other optical and near-infrared spectral regions as a test of consistency of our results. We note that profiles of the alkali lines obtained on different occasions agree quite well in intensities and widths. Some discrepancies may be explained by the signal-to-noise ratio differences or variability of dust shell within the atmosphere of LP 944−20.

First, we reproduce the overall spectral distribution and profiles of spectral lines of strong absorption lines of rubidium and potassium. Second, we find the lithium abundance in the atmosphere of LP 944−20 by fitting a DUSTY model atmosphere to the Li 670.8-nm line profile in the observed spectrum. We find that the fit to the observed fluxes provides a cosmic value of lithium abundance and that analysis of the observed pEW also yields the same $\log N({\rm Li}) = 3.25 \pm 0.25$ dex.

Tinney (1998) determined a lithium abundance of $\log N({\rm Li}) = 0.0 \pm 0.5$ from analysis of the EW of the lithium resonance doublet. We can reproduce Tinney's (1998) result if we use pEW as EW (see Section 4.4), as Tinney was forced to do by the then available atmospheric models. Indeed, only pEW of atomic lines can be measured in respect to the background formed by the haze of TiO lines (Pavlenko 1997a,b; Zapatero Osorio et al. 2002). The pEW values depend on the strength of the background molecular bands of TiO, on the spectral resolution of the data and on other broadening parameters (see Martín et al. 2005 for an example of how rotation affects the EWs of K I resonance lines). Reducing the TiO absorption in the region across the 670.8-nm line increases the relative strength of the computed Li lines and the formally determined lithium abundance decreases.

It is worth noting that we get some problems with fits of theoretical spectra computed for the conventional, i.e. self-consistent, model atmosphere to the observed SED of LP 944−20. The shape and intensity of the TiO bands around the resonance line of lithium are not well matched by 'standard' models. Generally speaking, because of the low surface temperature and activity properties of LP 944−20, it might be surprising to obtain good fits for conventional models, given that LP 944−20 provides substantial evidence of stellar activity phenomena in its atmosphere (Hα and radio emission, strong X-ray flares). Our knowledge of these processes is far from complete even in the case of the Sun. Indeed, the presence of these phenomena is clear evidence of the vertical stratification of the LP 944−20 atmosphere. On the other hand, it is plausible that TiO is absent in the upper atmosphere of LP 944−20 due to depletion of Ti atoms into dust particles and/or complete dissociation of TiO due to higher temperature there.

To investigate the impact of different factors on our main result and in order to provide a better fit to the observed spectra of LP 944−20, we adopt a more sophisticated model atmosphere. Namely, we suggest the presence of clouds at the level above the photosphere and complete depletion of TiO in the outermost layers of the atmosphere of LP 944−20. We treat the opacity provided by the dusty clouds as scattering with power dependence on wavelength. From the comparison of observed and computed spectra we determine parameters of scattering clouds. The temperature–pressure dependence in our model atmosphere was taken from the DUSTY model atmosphere of the Lyon group, i.e. our SE model is not self-consistent. Even in the Sun (e.g. HOLMU, VLC, MAKKLE), the use of SE model atmospheres is well acknowledged (see references in Gibson 1970). SE model atmospheres are used to fit some observed features using theoretical spectra computed with modified model atmospheres.

In our case the appearance of a dusty shell in the SE model atmosphere and/or depletion of TiO should change the temperature structure of the outermost atmospheric layers. With our SE models we obtain considerably better fits between observational and synthetic spectra in terms of the TiO bands, alkali lines and SED. From

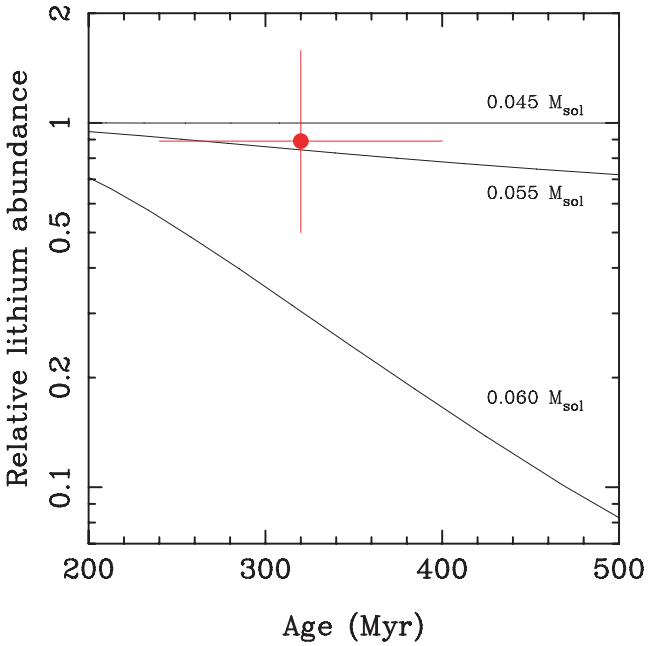

Figure 16. Location of LP 944−20 on the lithium depletion curves by Baraffe et al. (2003). We have adopted the age determination of Ribas (2003).

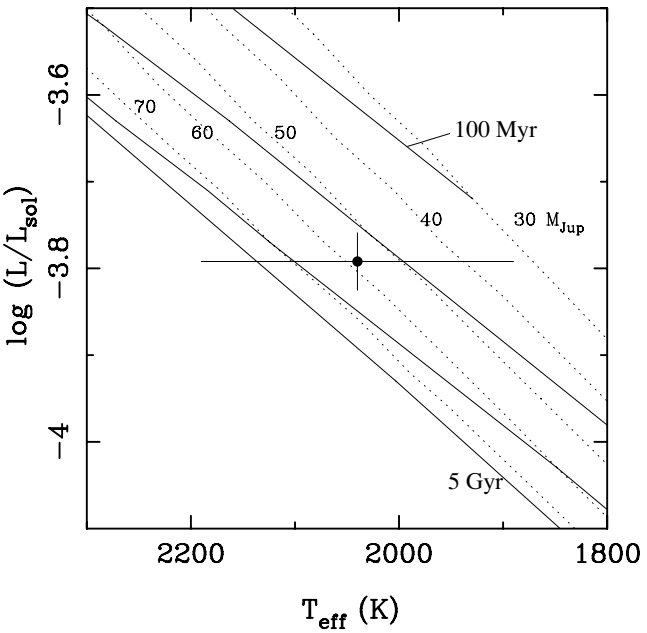

Figure 17. Location of LP 944−20 in the HR diagram and comparison with the evolutionary models of Baraffe et al. (2003). Isochrones (solid lines) correspond to the following ages: from top to bottom, 100, 300, 800 Myr and 5 Gyr. Evolutionary tracks (dotted lines) have masses labelled in Jovian units ($1\,M_{\odot} \sim 1000\,M_{\rm Jup}$).

fits to the Li resonance doublet we conclude that LP 944−20 has likely preserved all its original lithium content.

We also conclude that our lithium abundance shows a rather weak dependence on the input parameters of the models, despite the fact that our log N(Li) determination is carried out in the frame of LTE. Moreover, all the alkali lines fitted in our paper were computed in the frame of LTE. Fortunately, the alkali lines considered in this work are rather insensitive to chromospheric-like features (CLF) because processes of their formation are mainly controlled by photoionization (Thomas 1959). By definition, these lines should show a rather weak dependence on temperature structure of the outermost layers of atmosphere. Indeed, direct NLTE modelling of formation of lithium lines in the atmospheres of ultracool dwarfs with CLF shows their rather weak response to temperature inversions, in contrast to TiO lines (Pavlenko 1998a). Lithium lines can be affected only in the case of the strongest CLF producing additional flux in the blue part of the spectra, but that is unlikely in LP 944−20 given its age and level of Hα and X-ray activity.

Finally, comparison of our revised lithium abundance for LP 944−20 with the calculations of lithium depletion by Baraffe et al. (2003) shows a good agreement for a mass below 0.057 $M_{\odot}$ and an age of 320 ± 80 Myr (see Fig. 16). This result is marginally consistent with the earlier estimate of Tinney (1998), who derived a mass in the range 0.056−0.064 $M_{\odot}$. Using the same evolutionary models, we show that this age and a mass $\leqslant$0.057 $M_{\odot}$ are also consistent with the location of this brown dwarf in the Hertzsprung–Russell (HR) diagram (Fig. 17). Thus, our analysis supports the young age of a few hundred million years of LP 944−20 as suggested by Ribas (2003), and indicates a lower mass than previously reported in the literature.

ACKNOWLEDGMENTS

YVP's studies are supported the Royal Society and Leverhulme Trust. ELM acknowledges support from NSF research grant AST 02-05862, the Michelson Science Centre and Spanish MEC grant AYA2005-06453. We thank Isabelle Baraffe for providing evolutionary models upon our request. We thank Chris Tinney for the helpful comments. We are grateful to the user support group of the VLT. The W.M. Keck Observatory is operated as a scientific partnership between the California Institute of Technology, the University of California and NASA. The observatory was made possible by the generous financial support of the W.M. Keck Foundation. We extend our special thanks to those of Hawaiian ancestry on whose sacred mountain we are privileged to be guests. This research has made use of the SIMBAD data base, operated at CDS, Strasbourg, France.

REFERENCES

Allard F., Hauschildt P. H., Alexander D. R., Tamanai A., Schweitzer A., 2001, ApJ, 556, 357
Allard M. F., Allard F., Hauschildt P. H., Kielkopf J. F., Machin L., 2003, A&A, 411, L473
Anders E., Grevesse N., 1989, Geochim. Cosmochim. Acta, 53, 197
Andretta V., Gomez M. T., Severino G., 1991, Sol. Phys., 131, 1
Bailer-Jones C. A., Lamm M., 2003, MNRAS, 339, 477
Baraffe I., Chabrier G., Barman T. S., Allard F., Hauschildt P., 2003, A&A, 402, 711
Basri G., Mohanty S., Allard F., Hauschildt P. H., Delfosse X., Martín E. L., Forveille T., Goldman B., 2000, ApJ, 538, 363
Berger E. et al., 2001, Nat, 410, 338
Bihain G., Rebolo R., Bejar V. J. S., Caballero J. A., Bailer-Jones C. A. L., Mundt R., Acosta-Pulido J. A., Manchado Torres A., 2006, A&A, 458, 805
Burgasser A. J., 2001, PhD dissertation, California Institute of Technology
Burrows A., Volobuyev M., 2003, ApJ, 583, 985
Burrows A. et al., 1997, ApJ, 491, 856
Burrows A., Burgasser A. J., Kirkpatrick J. D., Liebert J., Milson J. A., Sudarsky D., Hubeny I., 2002a, ApJ, 573, 394
Burrows A., Ram S. R., Bernath P., 2002b, ApJ, 577, 986

Burrows A., Sudarsky D., Hubeny I., 2006, ApJ, 640, 1063
Caballero J. A., Béjar V. J. S., Rebolo R., 2003, in Martín E. L., ed., Proc. IAU Symp. 211, Brown Dwarfs. Astron. Soc. Pac., San Francisco, p. 455
Chabrier G., Baraffe I., 2000, ARA&A, 38, 337
Chabrier G., Baraffe I., Allard F., Hauschildt P., 2000, ApJ, 542, L19
Clarke F. J., Oppenheimer B. R., Tinney C. G., 2002, MNRAS, 335, 1158
Dahn C. C. et al., 2002, AJ, 24, 1170
Dlugach Zh. M., Mischenko M. I., 2005, Sol. Syst. Res., 39, 102
Dulick M., Bauschlincher C. W., Burrows A., 2003, ApJ, 594, 651
Ferguson J. W., Alexander D. R., Allard F., Barman T., Bodnarik J. G., Hauschildt P. H., Heffner-Wong A., Tamanai A., 2005, ApJ, 623, 585
Gelino C. R., Marley M. S., Holzman J. A., Ackerman J. S., 2001, preprint (astro-ph/0106062)
Gibson E. G., 1970, The Quite Sun. STIO NASA, Washington, p. 1
Granovsky A. A., 1999, http://classic.chem.msu.su./gran/gamess/index.html
Granovsky A. A., 2004, http://quantum-2.chem.msu.ru/gran/gamess/index.html
Gray D. F., 1976, The Observation and Analysis of Stellar Photospheres. Wiley-Interscience, New York, p. 484
Guenther E. W., Wuchterl G., 2003, A&A, 401, 677
Gurvitz L. V., Weitz I. V., Medvedev V. A., 1989, Thermodynamic Properties of Individual Substances. Science, Moscow
Hambaryan V., Staude A., Schwope A. D., Scholz R.-D., Kimeswenger S., Neuhaus R. E., 2004, A&A, 415, 265
Hayashi C., Nakano T., 1963, Prog. Theor. Phys., 30, 460
Helling C., Klein R., Woitke P., Nowak U., Sedlmayr E., 2004, A&A, 423, 657
Irwin P. G. J., Sihra K., Bowles N., Taylor F. W., Calcutt S. B., 2005, Icarus, 176, 255
Jones H. R. A., Tsuji T., 1997, ApJ, 480, 39
Jones H. R. A., Longmore A. J., Allard F., Hauschildt P. H., Miller S., Tennyson J., 1995, MNRAS, 277, 767
Jones H. R. A., Pavlenko Y., Viti S., Tennyson J., 2002, MNRAS, 330, 675
Jones H. R. A., Pavlenko Ya. V., Viti S., Barber R. J., Yakovina L. A., Pinfield D., Tennyson J., 2005, MNRAS, 358, 105
Kenworthy M. A., Parry I. R., Taylor K., 2001, PASP, 113, 215
Kirkpatrick J. D. et al., 1999, ApJ, 519, 802
Koen C., Matsunaga N., Menzis J., 2004, MNRAS, 354, 476
Kumar S. S., 1962a, Inst. for Space Studies. Rep., No. X-644-62-78, 1
Kumar S. S., 1962b, AJ, 67, 579
Kupka F., Piskunov N., Ryabchikova T. A., Stempels H. C., Weiss W. W., 1999, A&AS, 138, 119
Kurucz R. L., 1993, CD-ROM No. 1–23. Harvard-Smithsonian Observatory, Cambridge, MA
Lambert D. L., Luck R. E., 1976, Observatory, 96, 100
Lambert D. L., Mallia E. A., 1968, MNRAS, 140, 13
Leggett S. K., Allard F., Geballe T. R., Hauschildt P. H., Schweitzer A., 2001, ApJ, 548, 908
Liebert J., Kirjpatrick D., Cruz K. L., Reid I. N., Burgasser A., Tinney C. G., Gizis J. E., 2003, ApJ, 125, 343
Luhman K. L., 1999, ApJ, 525, 466
Luyten W. J., Kowal C. T., 1975, Proper Motion Survey with 48 Inch Schmidt Telescope. XLIII. One Hundred and Six Faint Stars with Large Proper Motion. University of Minnesota, Minneapolis
McGovern M. R., Kirkpatrick J. D., McLean I. S., Burgasser A. J., Prato L., Lowrance P. J., 2004, ApJ, 600, 1020
Magazzù A., Martín E. L., Rebolo R., 1993, ApJ, 404, L17
Martín E. L., Bouy H., 2002, New Astron., 7, 595
Martín E. L., Rebolo R., Zapatero Osorio M. R., 1996, ApJ, 469, 706
Martín E. L., Basri G., Delfosse X., Forveille Th., 1997, A&A, 327, L29
Martín E. L., Delfosse X., Basri G., Goldman B., Forveille Th., Zapatero Osorio M. R., 1999, AJ, 118, 2466
Martín E. L., Zapatero Osorio M. R., Lehto H., 2001, ApJ, 557, 822
Martín E. L., Magazzù A., García López R., Randich S., Barrado y Navascués D., 2005, A&A, 429, 1051
Martín E. L., Guenther E., Zapatero Osorio M. R., Bouy H., Wainscoat R., 2006, ApJ, 644, L75
Mohanty S., Basri G., 2003, ApJ, 583, 451
Mohanty S., Basri G., Jayawardhana R., Allard F., Hauschildt P., Ardila D., 2004, ApJ, 609, 854
Morel T., Micela G., Favata F., Katz D., Pillitteri I., 2003, A&A, 412, 495
Nakajima T., Oppenheimer B. R., Kulkarni S. R., Golimowski D. A., Matthews K., Durrance S. T., 1995, Nat, 378, 463
Pavlenko Y. V., 1997a, Astron. Rep., 41, 537
Pavlenko Ya. V., 1997b, Ap&SS, 253, 43
Pavlenko Ya. V., 1998a, Astron. Rep., 42, 501
Pavlenko Ya. V., 1998b, Astron. Rep., 42, 787
Pavlenko Ya. V., 2000, Astron. Rep., 44, 219
Pavlenko Ya. V., 2001, Astron. Rep., 45, 144
Pavlenko Ya. V., 2005, Astron. Nachr., 326, 934
Pavlenko Ya. V., Jones H. R. A., 2002, A&A, 396, 967
Pavlenko Y. V., Rebolo R., Martín E. L., García López R. J., 1995, A&A, 303, 807
Pavlenko Y., Zapatero Osorio M. R., Rebolo R., 2000, A&A, 355, 245
Pavlenko Ya. V., Jones H. R. A., Lyubchik Y., Tennyson J., Pinfield D. J., 2006, A&A, 447, 709
Pavlenko Ya. V., Zhukovska S., Volobuyev M., 2007, Astron. Rep., 51, 282
Plez B., 1998, A&A, 337, 495
Rebolo R., Martín E. L., Magazzu A., 1992, ApJ, 389, L83
Rebolo R., Zapatero-Osorio M. R., Martín E. L., 1995, Nat, 377, 129
Rebolo R., Martín E. L., Basri G., Marcy G. W., Zapatero-Osorio M. R., 1996, ApJ, 469, L53
Ribas I., 2003, A&A, 400, 297
Rutledge R. E., Basri G., Martín E. L., Bildsten L., 2000, ApJ, 538, 141
Stelzer B., 2005, Mem. Soc. Astron. Ital., 76, 410
Thomas R. N., 1959, ApJ, 125, 260
Tinney C. G., 1998, MNRAS, 296, L42
Tinney C. G., Reid I. N., 1998, MNRAS, 301, 103
Tinney C. G., Tolley A. J., 1999, MNRAS, 304, 119
Tsuji T., 1973, A&A, 23, 411
Tsuji T., 2002, ApJ, 575, 264
Tsuji T., Ohnaka K., Aoki W., Nakajima T., 1996, A&A, 308, L29
Unsöld A., 1955, Physik der Sternatmospharen. Springer-Verlag, Berlin
Viti S., Jones H. R. A., 1999, A&A, 351, 1028
Zapatero Osorio M. R., Béjar V. J. S., Pavlenko Y., Rebolo R., Allende Prieto C., Martín E. L., Garcia Lopez R. J., 2002, A&A, 384, 937
Zapatero Osorio M. R., Lane B. L., Pavlenko Y., Martín E. L., Britton M., Kulkarni S. R., 2004, ApJ, 615, 958
Zapatero Osorio M. R., Martin E. L., Bouy H., Tata R., Deshpande R., Wainscoat R. J., 2006, ApJ, 647, 1405

This paper has been typeset from a TEX/LATEX file prepared by the author.